Pore Space Characterization of Carbonated Binary Micro-Computed Tomography Images, Case Study

Ashrafi, Mohammad
Sahand University of Technology, Tabriz, I.R. IRAN

Tabatabaei-Nezhad, Seyyed Ali Reza**+; Khodapanah, Elnaz
Faculty of Petroleum and Natural Gas Engineering, Sahand Oil and Gas Research Institute (SOGRI), Sahand University of Technology, Tabriz, I.R. IRAN

ABSTRACT: *Pore space characterization helps a better understanding of porous media. The pore geometry and topological properties in carbonated rocks are important for a better understanding of the complex hydrologic and elastic properties. A detailed model of the pore space constructed directly from three-dimensional images can bring reliable results because the porous media complexity would be considered. In this study, by considering different methods a deep understanding of some carbonated pore spaces is obtained. Four series of 2D micro-computed tomography binary images for carbonated rock have been collected, and each of them was considered as a 3D binary image. Using novel skeletonization and pore-throat segmentation algorithms, some network properties have been evaluated and compared for the four cases. Those considered properties were pore and grain size distribution, throat length frequency, and coordination number frequency. Moreover, the geometric measures in 2D and 3D have been considered using Minkowski functionals. The area, the perimeter, and the 2D Euler number of 2D binary images and the volume, the surface area, and the mean breadth which is also known as the integral of the mean curvature and the 3D Euler Number of the 3D binary images are also considered.*

KEYWORDS: *Pore network characterization; Carbonated rock; 3D Binary Image; Skeletonization; Skeleton to graph algorithm.*

INTRODUCTION

Carbonated rocks such as dolomite and limestone are characterized by their extremely low porosity and permeability. The presence of a very small amount and different types of void spaces influences the characteristics of carbonated rocks. Therefore, a comprehensive understanding of the pore-throat distribution, topology, and geometry in carbonated rocks is necessary for their quality evaluation.

Different techniques can be used for characterization of carbonated rocks. For example, the pore size distribution can be characterized by various techniques. These are thin section analysis, Scanning Electron Microscopy (SEM), X-ray Computed Tomography (CT), Pressure-Controlled Porosimetry (PCP), Rate-Controlled porosimetry (RCP), Nuclear Magnetic Resonance (NMR)

* *To whom correspondence should be addressed.*
\+ *E-mail: tabalireza @yahoo.com & tabatabaei @sut.ac.ir*
1021-9986/2022/11/3816-3830 15/$/6.05

and N_2 adsorption. It should be noted that all these techniques have their own limitations.

The SEM and thin sections cannot provide quantitative data. PCP fails to take into account the large pores; RCP cannot reveal the distribution of tiny throats. CT is an expensive method and is associated with inevitable errors in calculating the pore-throat radius, and the NMR test range is limited by surface relaxivity [1].

Nowadays different techniques have been developed to characterize porous media [2-5]. Among these methods micro-computed tomography known as micro-CT imaging is the most referred one [6]. When proper images of rocks are available, characterization becomes possible in an indirect manner through finding the relationship between the image properties and the desired specification of rock.

Depending on what is considered to be a pore and/or throat, a pore network can be constructed directly from the images. Pore network robustness depends on the way of partitioning the real void space into pores and throats [7]. Also location, size and shape of pores and throats influence network properties. The closer the pore network to the real porous media, the better the network will be.

There are three void space representation methods [8], first, creation void spaces considering the sedimentary process through which rock is formed, second, statistically equivalent network generation using distributions of basic morphologic parameters and third, direct micro-CT imaging from a real sample to yield an irregular lattice [9]. These networks can help to better characterize porous media.

Image analysis to extract pores and throats size distributions and their connectivity can provide more details for researcher about the pore spaces [7]. The medial axis-based algorithms create an image skeleton. Throats are located at local minima and pores are placed at the skeleton nodes [10,11]. Skeleton properties can also bring more details on pore and throats.

Pore topology can be shown by standard parameters. The standard parameters used in quantitative analysis of spatial structures are area and perimeter in 2D, and volume, surface area and mean breadth in 3D. Another parameter is the Euler-Poincaré characteristic, these parameters form the so-called Minkowski functionals can be evaluated. The Euler-Poincaré characteristic is a standard connectivity parameter that for a planar structure is equal to the number of its connected components minus the number of holes [12].

Euler number (χ) depends on the reconstruction number (#) of vertices (V), edges (E), faces (F) or solids (S), given by Equation 1, the classical Euler formula.

$$\chi = \#\mathrm{V} - \#\mathrm{E} + \#\mathrm{F} - \#\mathrm{S} \quad (1)$$

The approximation of the Euler-Poincaré measure strongly depends on the choice of the adjacency system. Different adjacency systems yield very different results. One possibility is to choose the adjacency system depending on the geometry of the structure. For example, one can choose 4-adjacency or 6-adjacency for thick structures, and 8-adjacency or 26-adjacency for structures having thin edges.

THEORETICAL SECTION

Permeability from geometric and topological properties

If characterization is conducted well on the samples, petrophysical properties can be achieved using the properties derived during the characterization. A review on the methods that consider geometric or topological properties to get absolute permeability is described in the following to show the importance of calculating network parameters such as grain radius and geometric parameters like Euler number.

Absolute permeability represents the ability of a porous medium to conduct fluid flow. It is usually measured through core flooding experiments and calculated from Darcy's Law as Eq. (2).

$$\mathrm{K} = \frac{\mathrm{Q}\mu\mathrm{L}}{\mathrm{A}\Delta\mathrm{P}} \quad (2)$$

Where, K is absolute permeability, Q is flow rate, μ is fluid viscosity, L is length of the sample, A is cross-sectional area and ΔP is pressure gradient.

The Carman-Kozeny given by Eq. (3) is a well-known empirical equation through which permeability is correlated with rock porosity. A commonly used approximate permeability-porosity relation is the Kozeny-Carman equation, expressed by Eq. (4).

$$\mathrm{K} = \frac{\phi \mathrm{r}^2}{8\tau} \quad (3)$$

$$\mathrm{K} = \frac{1}{72}\frac{\phi^3}{(1-\phi)^2}\frac{1}{\tau^2}\mathrm{D}^2 \quad (4)$$

Where, ϕ is rock porosity, r is effective radius and τ is tortuosity, D denotes the grain diameter. This model assumes that a porous medium can be represented

as a solid block permeated by parallel cylindrical pipes. The proportionality constant 1/72 is sometimes replaced by a fitting parameter.

Another widely used empirical correlation is the Katz-Thompson model as given by Equation 5, the term σ/σ_0 in Eq. (5) can be linked to the porosity according to Archie's law as represented by Eq. (6) [13].

$$K = {cl_c}^2 \frac{\sigma}{\sigma_0} \quad (5)$$

$$\frac{\sigma}{\sigma_0} = \frac{(\phi - \phi_c)^z}{(1 - \phi_c)} \quad (6)$$

Where, c is the constant equals to 1/226, l_c is characteristic length of the pore space, σ is conductivity of rock saturated with a brine solution of conductivity σ_0, ϕ_c is porosity at the percolation threshold and z is the critical exponent. Because electrical conductivity is influenced by topology of the pore space this relationship implicitly captures pore topology while the geometry of the pore space is obtained from the characteristic length term.

The Katz-Thompson model (Eq. (5)) has been further developed by replacing the σ/σ_0 term with parameters related to the pore morphology. The new formulated equation is represented by Equation 7 and referred to as Scholz's model [13].

$$K = {cl_c}^2 \left(\frac{1 - \chi_0}{N}\right)^{\alpha} \quad (7)$$

Where, χ_0 is Euler characteristic of the conducting phase and N is number of grains in granular porous media. For a 2D geometry c=1/12 and α is a free parameter for which the best agreement is found as α=1.27.

Scholz proposed the effective grain number ($\widehat{N}$) be replaced by N as below [13].

$$\widehat{N} = \frac{P^2}{4\pi A\phi} - \frac{\chi}{\phi} \quad (8)$$

Where, P is perimeter and A is the area.

Heuristic models for estimating the 3D permeability from the Lattice Boltzmann computed 2D permeabilities have been presented by Saxena. It is clear that no single approach can yield a perfect 2D to 3D transformation, since the solution of this problem is fundamentally non unique, given that the same 2D micro structures can be cut from many different 3D composites. Saxena proposed two models, including the Kozeny-Carman approach (Model 1) and the Flow path deviation approach (Model 2) [14].

Using the first model, the Kozeny-Carman expression for permeability can also be expressed by Eq. (9) [14].

$$K \approx \frac{1}{2} \frac{\phi^3}{\tau^2 {S_0}^2} \quad (9)$$

Where S_0 is the specific surface area. Hence, Eq. (10) can be derived [14].

$$\frac{K_{3D}}{K_{2D}} \approx \frac{S_{2D}^2}{\tau_{3D}^2 S_{3D}^3} \quad (10)$$

For an arbitrary packing of identical spherical grains in 3D, the specific surface area is $S_{3D} = 3(1 - \phi)/R$, where R is the sphere radius. Similarly, the specific surface area for an arbitrary packing of parallel circular cylinders is given by $S_{2D} = 2(1 - \phi)/R$, where R is the cylinder radius.

Saxena used a model for porosity dependent tortuosity given by Eq (11) [14].

$$\tau_{3D} \approx 1 - p\log\phi \quad (11)$$

Where, p is an empirical parameter (p = 0.41 for sphere packs; p = 0.63 for cubes). Therefore, the estimated 3D permeability is given by Eq. (12) [14].

$$K_{3D} \approx \frac{4}{9} \frac{K_{2D}}{(1 - p\log\phi)^2} \quad (12)$$

Model 1 does not incorporate the effects of change in flow field from pipes of constant diameter in 2D to variable diameter in 3D. Thus, *Saxena* considered another approach that accounts for sinusoidally changing pore diameter in 3D along with distortion of pipe diameter upon slicing. The final expression for model 2 is given by Eq. (13) [14].

$$K_{3D} \approx 0.24 \frac{1}{1 - \bar{\delta}} \sqrt[4]{2\left(1 - \bar{\delta}^2\right)^{\frac{7}{5}}} \frac{}{2 + 3\bar{\delta}^{-2}} \times \left(1 + \frac{16\pi^2}{3} \frac{\bar{\delta}^{-2}}{\bar{\lambda}^{-2}} \frac{\left(1 - \bar{\delta}^2\right)}{2 + 3\bar{\delta}^{-2}}\right)^{-1} K_{2D} \quad (13)$$

Where, $\bar{\delta}$ is the normalized magnitude of variation in radius, and $\bar{\lambda}$ is the variation in wavelength. The factor 0.24 accounts for distortion of tube diameter upon slicing in all possible directions.

Model parameters p and δ depend on the details of rock microstructure. It is found that parameters p and δ sharply decline with increase in porosity, and are well described by the following empirical relations [14].

$$p = 3e^{-7\phi} \quad (14)$$

$$\delta = e^{-9\phi} \quad (15)$$

The dependency of topological and geometrical properties on petrophysical properties is obvious from the above equations, which has been studied by different researchers. This study is focused on the characterization of four carbonated rocks using their micro CT binary images.

The conducted study presents a rational approach to obtain the petrophysical and topological properties from micro samples of porous media property. Often large size plugs or core samples of porous media are not available, for example, rock cutting comes out a hole by drilling mud. In those situation where there are small pieces of porous material, use of proper image acquisition methods following by characterization procedure explained in the next section, can help to obtain a great understanding from small pieces. The characterization procedure is a combination of topological Minkowski functionals and recently proposed pore network extraction methods along with some improvement which have been applied on micro CT binary images.

Methods

Different types of direct imaging methods are available to describe rock materials. Micro-CT imaging is an accurate and repeatable method for evaluating the pore system and can be conducted on plug, core, sidewall core, drill cuttings and outcrops.

Despite a large amount of available information, the actual three-dimensional grain relationships and details of the inter granular pore structure are always beyond our reach. While digital image analysis is not novel, important recent advances are available in petrography including pattern recognition and pattern classification software for description and quantification of rock geometric characteristics. These approaches started by development of the arena of pore image analysis to determine the size, shape and relative proportions of different pore types through computer based thin section porosity analysis. It is possible to define many variables for each field of view using this technique.

It is far beyond the scope of this research to even begin an analysis of the applications of image analysis to geological samples. However, providing some discussion is reasonable in the context of analyzing and quantifying pore structures

A key requirement of many forms of pore structure image analysis is that they require binary images that show pore and grain spaces. These are typically obtained by thresholding greyscale images.

Note that even for a simple system the process of image segmentation does not necessarily yield a unique solution for which there are several reasons. First, the background, considered here as the grey-scale level may not be flat across the image. This is often a function of the instrument settings and must be corrected before thresholding or segmentation.

Selecting the appropriate method for segmenting an image is of great importance, either for simply choosing a threshold for a 2D or 3D image or using a more complex segmentation approach. Given the complexity of this issue, careful examination and comparison of various approaches are clearly beyond the scope of this review, however, it is important to note that there are a large number of algorithms for selecting a threshold.

Visualization of 3D network

Rabbani et al. have been developed some codes that can visualize 3D binary images. Their code can be implemented on either grains or pores to segment them. Following that, grain and pore size distributions become available. Knowing properties including size and location, relationships between pores, called throat, are determined and finally pore network model can be extracted by the Rabbani method [15].

To illustrate the network from known pore and throat properties, a code has been written by authors which is implemented on the network extracted using the Kollmannsberger method [16-17].

The Kollmannsberger method has been originally introduced and applied in bone image processing and the current work is the first time of its usage in rock imaging context. It is worth mentioning that Rabbani's method assumes spherical pore shapes while the Kollmannsberger method can consider any pore shape. Moreover, since the Kollmansberger method, in contrast to Rabbani method, doesn't contain a visualization procedure, we developed a code for this purpose, the results of which are given in this paper.

Skeleton and skeleton to graph calculation

By using the skeletonization algorithm and the skeleton to graph algorithm that was claimed to be able to distinguish

pores and throats for a 3D binary skeleton, the pore properties of carbonated micro CT images have been obtained. Here, 1-voxel of binary image is assigned to void spaces while 0-voxel is assigned to grains. A new skeletonization algorithm and skeleton to graph algorithm have been proposed similar to Kollmannsberger [16-17]. The methods need two inputs, the 3D binary matrix, and a threshold for the minimum length of branches, to filter out skeletonization artifacts. The threshold is considered one in all the extracted networks studied in this paper. The pore network can be built by a combination of skeletonization and skeleton to graph algorithms. Then, the pore size distribution, throat length frequency and coordination number for the network can be evaluated. Also, grain size distribution can be obtained using the method proposed by *Rabbani* [15].

Several methods can be employed to directly measure rock properties. For example, rock porosity can be measured directly by saturation or imbibition, buoyancy, gas expansion, gas adsorption and mercury intrusion porosimetry. All five methods only measure the effective porosity of the rock sample. Using micro CT images, all kinds of porosities can be estimated.

Geometric properties calculation

Minkowski geometric measure parameters for 2D images are the area, the perimeter and the (2D) Euler Number and for 3D images parameters are the volume, the surface area (called surface), the mean breadth (also known as integral of mean curvature) and the (3D) Euler Number [12].

The area of object in binary image corresponds roughly to the total number of on(one) pixels in the image, but may not be exactly the same because different patterns of pixels are weighted differently. An algorithm estimates the area of all of the on pixels in an image by summation of the areas of each pixel in the image. A single on pixel surrounded by off(zero) pixels has a total area of 1. Number of objects is the number of connected components (objects) in binary image. The connectivities of 4 and 8 for two dimensions; and 6, 18 and 26 for three dimensions can be considered to evaluate geometric measures parameters.

The Euler number for the 2D binary image is a scalar whose value equals to the total number of objects in the image minus the total number of holes in those objects. 4-connected objects and 8-connected objects can be considered in 2D. A pixel is a part of the perimeter; if it is nonzero and connected to at least one zero valued pixel. The connectivity can be 4 or 8 for two dimensions, and 6 or 18 or 26 for three dimensions [12].

RESULTS AND DISCUSSION

Studied cases

Network properties are investigated for four micro CT binary images. C1 and C2 are carbonated dolomite rocks, and Est and Kett are carbonated limestone rocks [18-19]. For each case, the series of 2D images that create a 3D image were available. One slice of each case is depicted in Fig. 1. The sizes and resolutions of the images of the studied carbonated rocks are different. The Kett image is larger than the other three ones. However, all cases have resolutions close to each other as shown in Table 1. Porosities and reported absolute permeabilities are also given in Table 1. The highest porosity and the highest permeability values are obtained for the C1 and the lowest permeability value is obtained for the C2. As Fig. 1 shows Kett has more circular grains than the others. Vuggy space and small inter granular void spaces can be observed in C1, C2 and Est. Fig. 2 is a 3D visualization of the four studied cases in which segmented pores have been illustrated by the Rabbani method [15]. Segmentation has been implemented by applying a watershed segmentation algorithm.

Porosities of the studied cases

For all of the studied cases, the total porosity is equal to summation of 1-voxels divided by total voxels number of the binary image. The number of connected 1-voxels regions are obtained for all cases as shown in Table 2. Those regions which consist of 1-voxels at the inlet and outlet simultaneously are counted as common regions. All cases are cubes. If a cube face is considered as inlet, the opposite face will be assumed as the outlet. Effective porosities can be calculated by summation of 1-voxels in common regions divided by total voxels number. In all the studied cases there was one common region. Skeletonization has preserved 1-voxels connectivity between the inlet and the outlet. Summation of 1-voxels for skeletons has been obtained and the skeleton porosities for all the studied cases are given in Table 2. C1 and C1 have high region numbers and skeleton porosities which it maybe because of their higher porosities.

Table 1: Carbonated rock image and petrophysical properties.

Name	Est	Kett	C1	C2
Permeability (mD)	59	172	785	38
Porosity (Fraction)	0.11	0.13	0.23	0.17
Size	650*650*650	1000*1000*1000	400*400*400	400*400*400
Resolution (Micron/Voxel)	3.3113	3	2.85	5.345

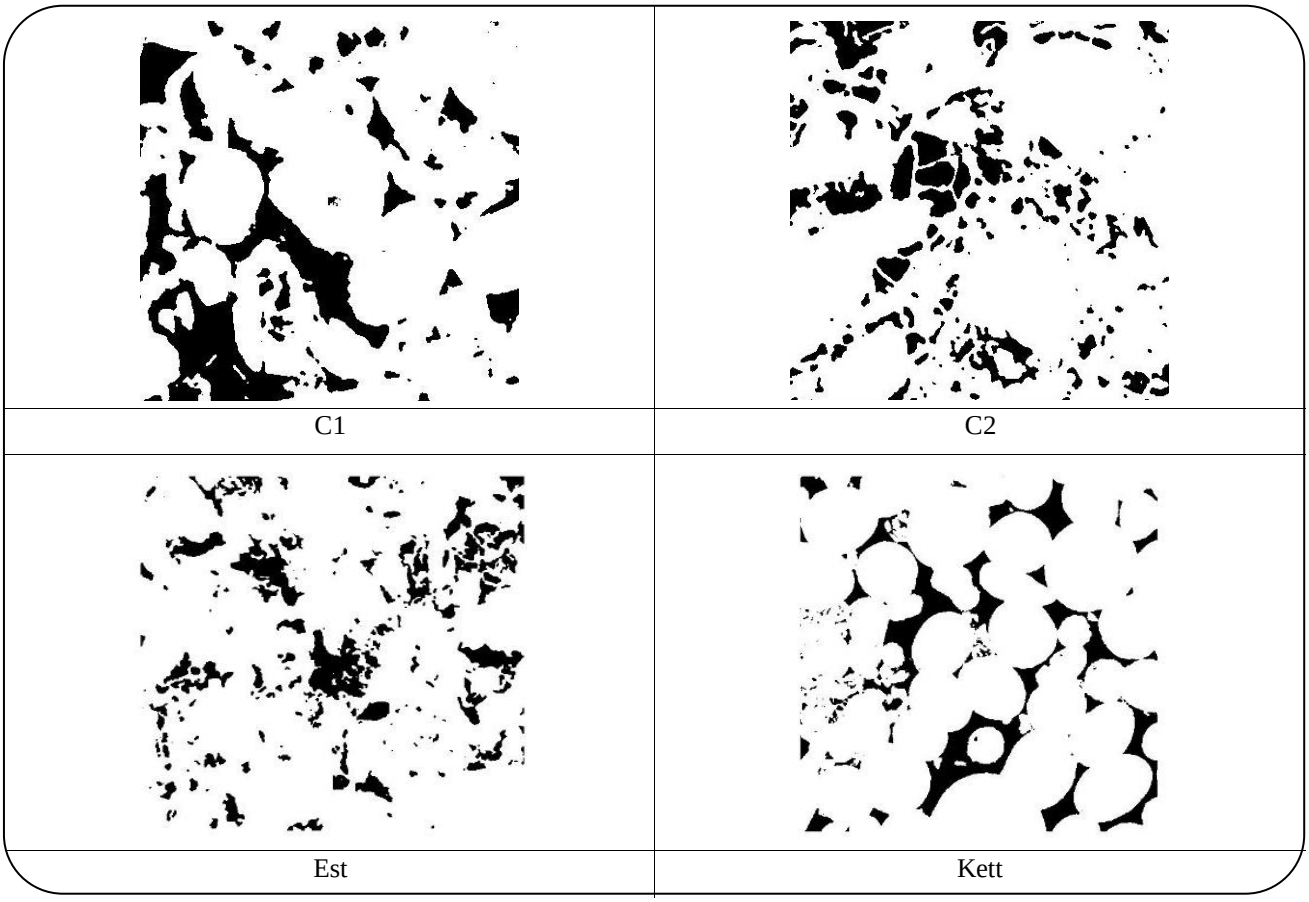

Fig. 1: First layer of binary images of the carbonate rocks, white color denotes grains and black denotes void spaces

Skeleton and graph properties

Skeletons were converted to network graph in a manner that all pores and throats characterization have been obtained using the algorithm proposed by *Kollmannsberger* [16-17]. According to *Mostaghimi et al.* in 2012, image size of 200 voxels on each side was considered for all the cases. Hence, the studied porous media was reduced to cube size of 200 which is the Representative Elementary Volume (REV) [20].

Also, pore size coordination number and throat length frequencies for each network were obtained. The largest pore size, average pore size, pores number, throats number, average throat length, maximum throat length, average coordination number and maximum coordination number were determined for all the cases, which is shown in Table 2. Therefore, a better sample characterization was achieved. The average pore radius of Est is larger than the other three cases which is reasonable considering the higher number of pores in C1 and C2. Kett has a lower number of throats compared with others samples which maybe because of its grain size uniformity. The porosity of C1 is higher than C2, hence, it is reasonable that

Table 2: Pore space properties of carbonated rocks.

Carbonated rock name	C2	C1	Kett	Est
Region Number	594	489	138	17
Skeleton Porosity	0.005727	0.004133	0.000907	0.001074
Biggest Pore Size (Voxel)	4195	1274	86	24
Second Big Pore Size (Voxel)	1937	1047	72	11
Third Big Pore Size (Voxel)	802	962	13	10
Average Pore Radius (micron)	24.4	11.7	22.7	29.4
Maximum Pore Radius (micron)	166	71.3	85.4	80.8
Pores Number	4423	3291	906	1132
Average Coordination Number	2.218856	2.20784	2.002208	1.952297
Throats Number	594	489	138	17
Average Throats Length (micron)	0.005727	0.004133	0.000907	0.001074
Maximum Throat Length (micron)	4195	1274	86	24
Average Grain Radius (micron)	1937	1047	72	11

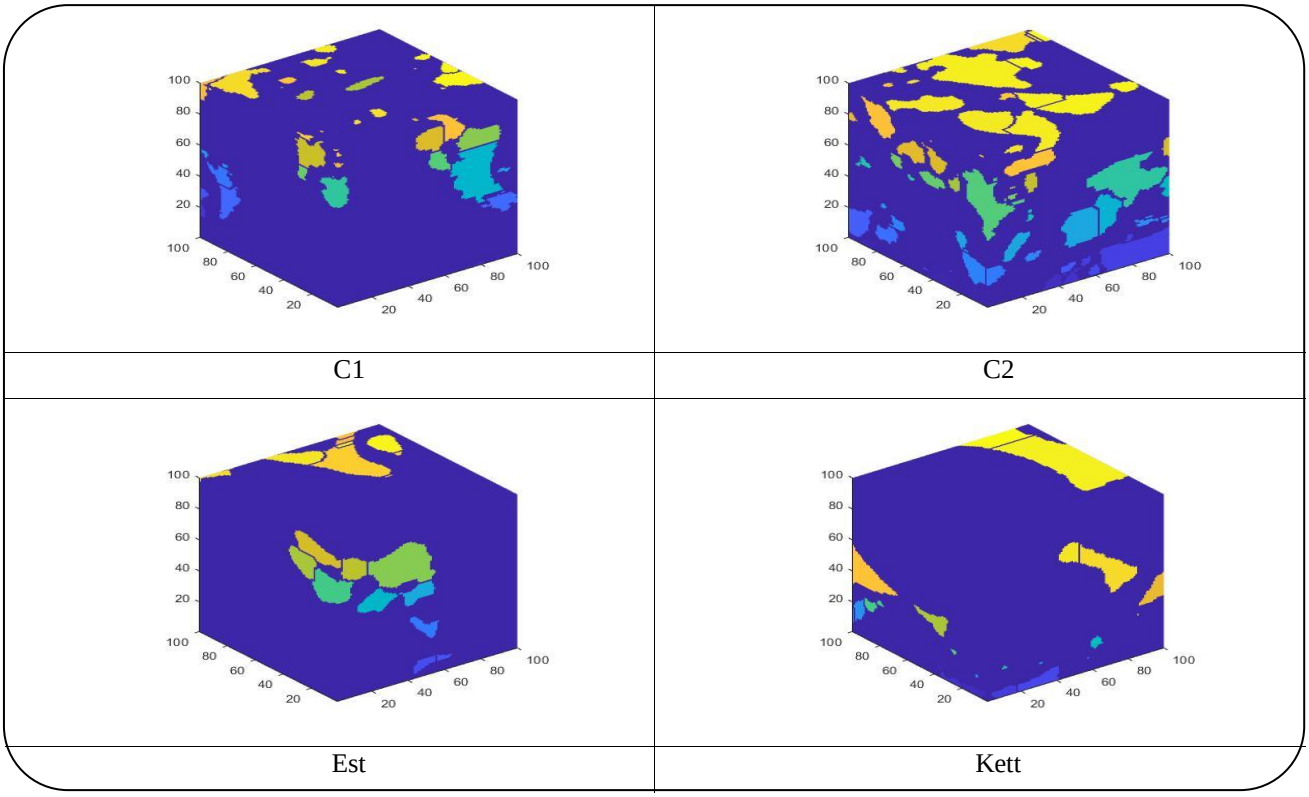

Fig. 2: 3D visualization of void space segmentation.

the lower average throat length has been obtained for C1 compared with C2.

After partitioning the void space into nodes and links similar to Kollmannsberger [16, 17], throat specification is obtained from links properties. The pore size distribution is obtained by skeleton nodes evaluation and binary images Euclidean distance transformation by which the volume of each pore is attained. Since, in contrast to Rabbani method, the Kollmannsberger method does not introduce a visualization procedure, in the present work codes have been developed which provides representation of the pore network. The pore size distribution trends,

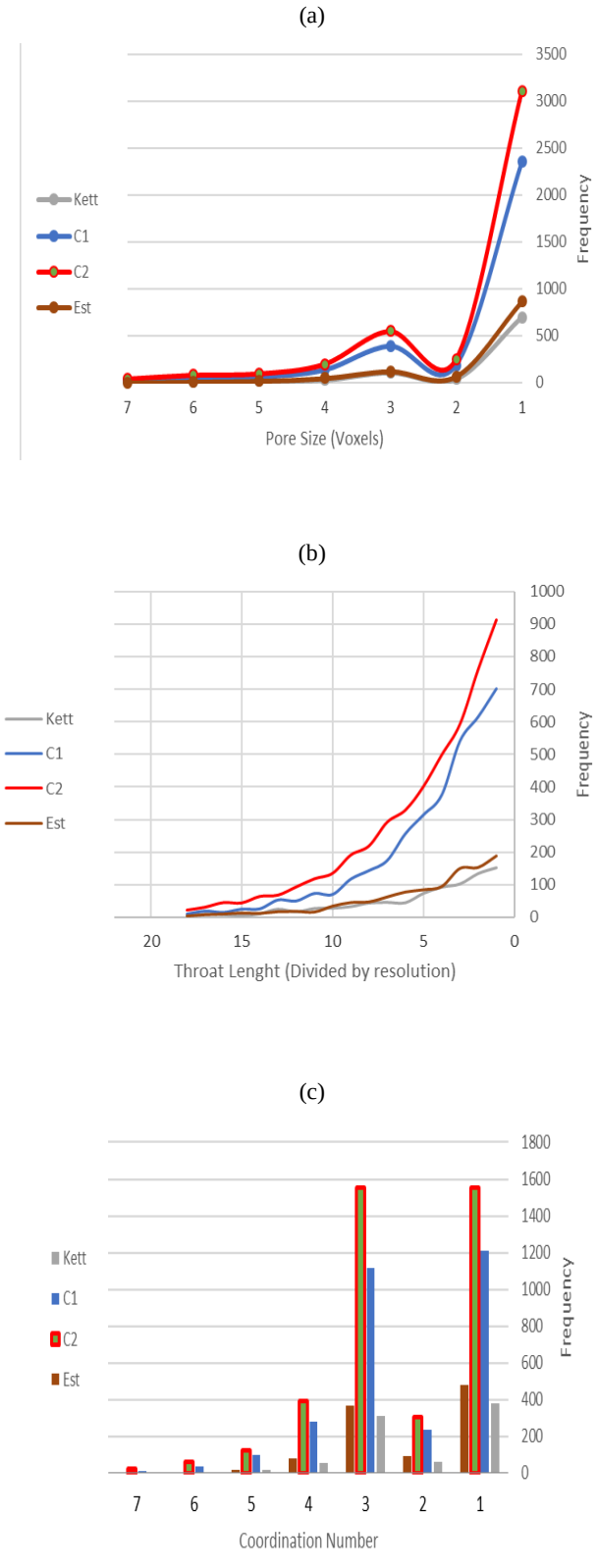

Fig. 3: Carbonated rocks networks' (a) pores size distribution, (b) throat length frequency, and (c) coordination number.

the throat length frequency curves and the coordination numbers are depicted in Fig. 3. The generated networks obtained using Kollmannsberger method considering the new developments are depicted in Fig. 4. As Fig. 4 shows, there are lower paths between two sides of the cube in Est and Kett rocks than those in C1 and C2. The generated networks obtained by Rabbani method are depicted in Fig. 5 in which pore and throat size are shown by color codes.

Samples grain size

Grain size distribution can be evaluated using the method proposed by *Rabbani* [15]. When *Rabbani* method is implemented to images depicted in Fig.1, Fig. 6 is created. The average grain radii for all the cases are shown in Table 2. The average grain size of Kett is higher than that of the other three rocks. 3D visualization of segmented grains obtained by Rabbani method are depicted in Fig. 7. The grain size distribution for all the four cases are obtained as Fig. 8 using the Kollmannsberger method regarding the developed method. Grain size distributions of carbonated rocks based on the networks obtained by the Kollmannsberger's method are shown in Fig. 8. Also, the pore and grain size distributions based on the networks shown in Fig. 5 have been calculated and illustrated in Fig. 9.

Minkowski functionals of the samples

To understand the geometric characteristics of carbonated rocks, the Minkowski functionals for three cases were conducted and shown in Table 3. Area, perimeter, Euler number and number of objects for 2D images and volume, surface, mean breadth, Euler number and number of objects for 3D images for all the possible connectivity systems have been obtained. As Table 3 shows, all 2D properties of C1 are lower than those of C2 and Est. This may be attributed to C1's higher permeability. Also, all 3D properties of C2 are higher than those of the other samples. Hence, roughly the higher the permeability, the higher the 2D geometric properties and the lower the 3D geometric properties. For each 2D binary layer of C1, C2 and Est porosity, Euler number, area and perimeter have been calculated and their frequencies are depicted in Fig. 10, Fig. 11 and Fig. 12 respectively. There are two humps in plots of porosity, area and perimeter frequencies of C1 and Est, indicating the double porosity behavior of carbonated rocks. In C2 there are three humps in those three frequencies plots. Also, the 2D Euler number frequencies have a similar behavior.

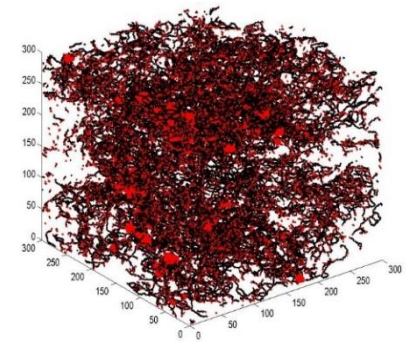

C1

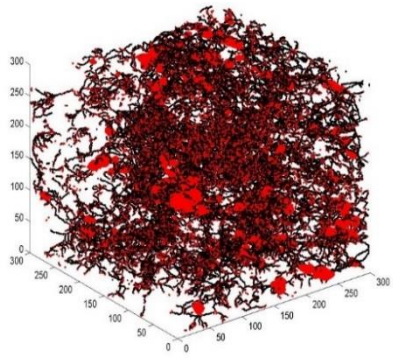

C2

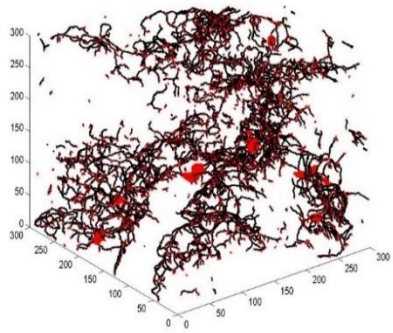

Est

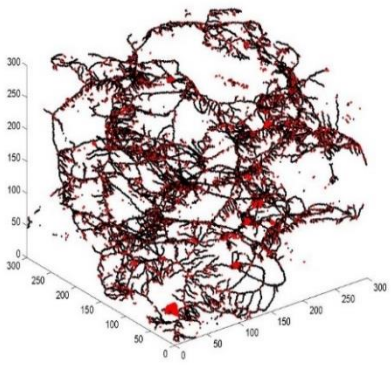

Kett

Fig. 4: Carbonated rocks pore networks obtained using Kollmannsberger method.

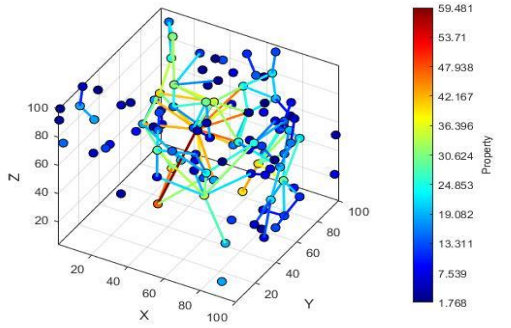

C1

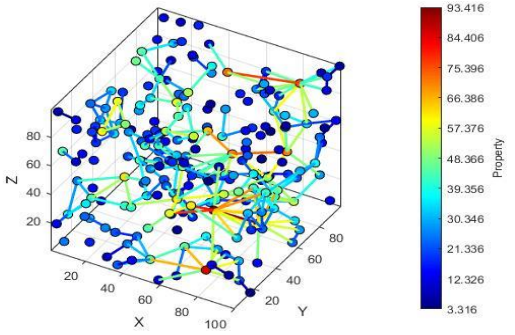

C2

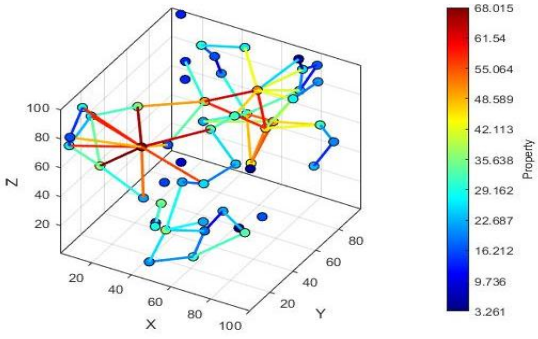

Est

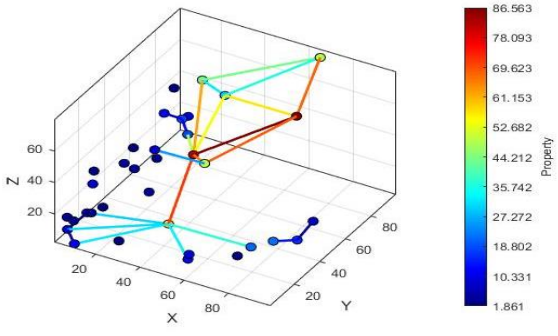

Kett

Fig. 5: Pore networks obtained using Rabbani method.

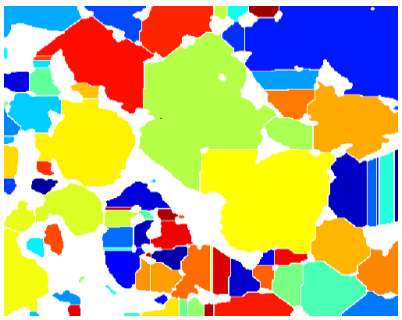

C1

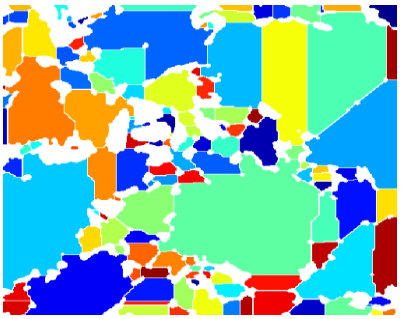

C2

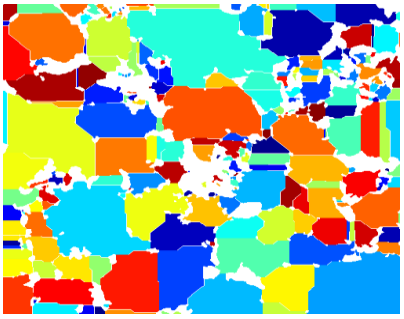

Est

Kett

Fig. 6: Segmented grain size of the first layer of carbonated rocks obtained by Rabbani method.

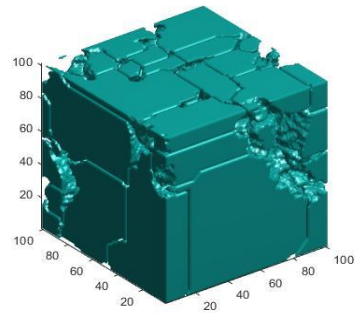

C1

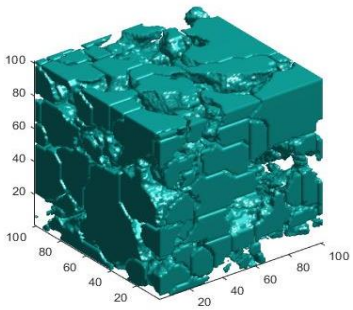

C2

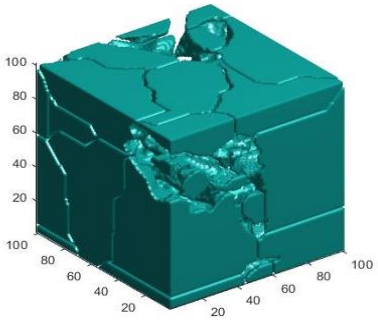

Est

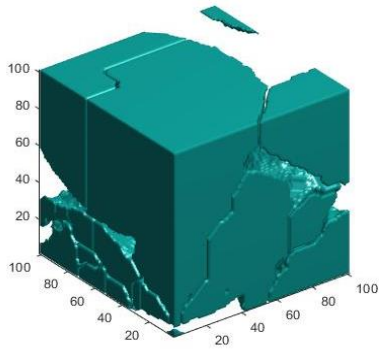

Kett

Fig. 7: 3D visualization of segmented grains.

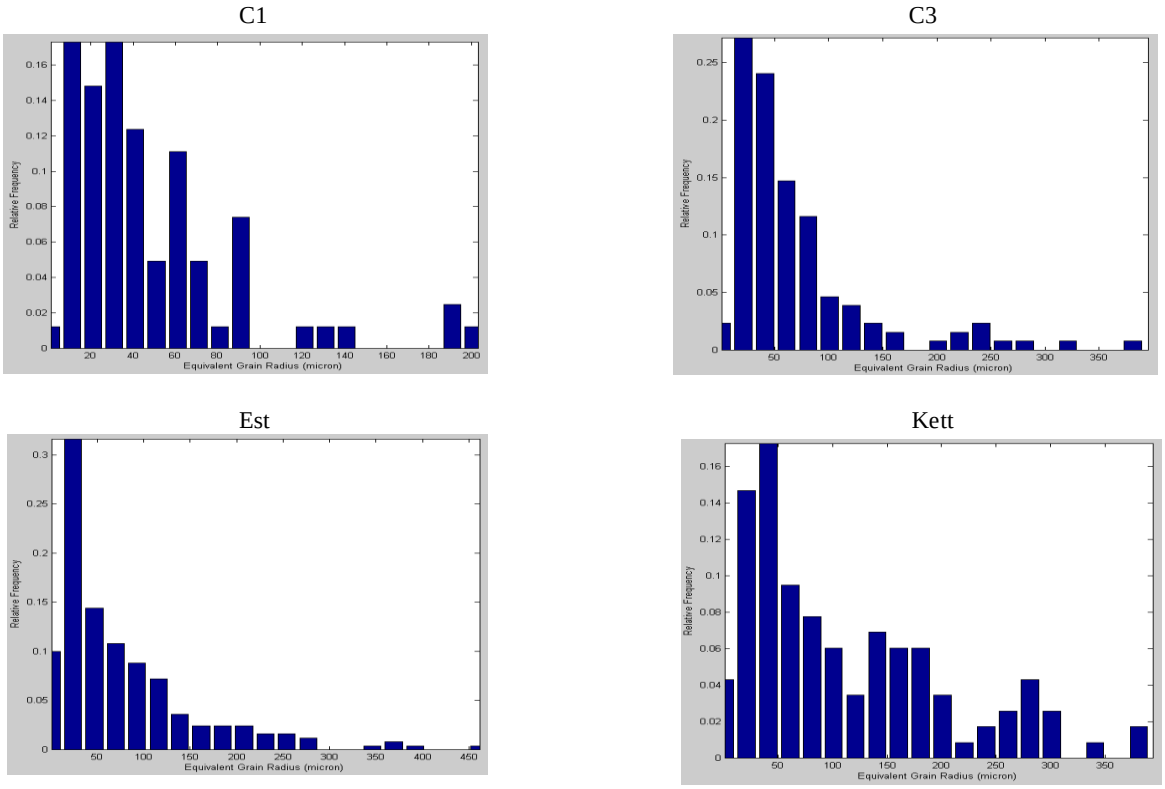

Fig. 8: Grain size distributions of carbonated rocks based on the networks obtained by the Kollmannsberger method.

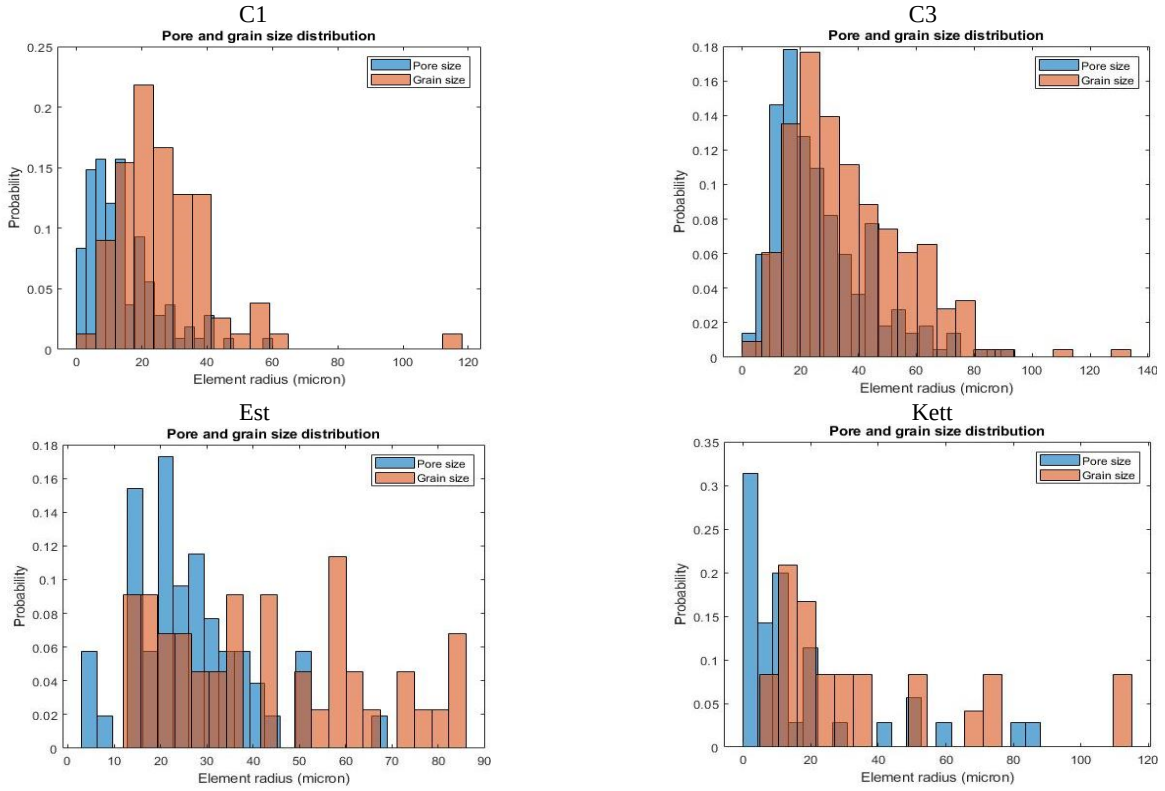

Fig. 9: Pore and grain size distribution by Rabbani's method.

Table 3: Values of geometric parameter for C1, C2 and Est.

Parameter	C1	C2	Est
2D area	302304.8	769341.8	599138.5
2D perimeter of 2 connectivity	21848.74	44008.8	35548.71
2D perimeter of 4 connectivity	21900.72	43927.85	36016.42
2D Euler number of 4 connectivity	86.305	177.6375	105.4185
2D Euler number of 8 connectivity	78.0675	168.1775	103.9323
2D number of objects of 4 connectivity	109.4325	195.94	121.2338
2D number of objects of 8 connectivity	104.0625	188.9325	120.1554
3D Volume	3.45E+08	1.64E+09	1.29E+09
3D surface of 3 paths	36647182	1.33E+08	99808211
3D surface of 13 paths	36960664	1.34E+08	1.02E+08
3D mean breadth of 3 path	143399.7	490731.6	237395.9
3D mean breadth of 13 path	143247.9	488673.6	246299.5
3D Euler number of 6 connectivity	152	2233	-4746
3D Euler number of 26 connectivity	-1362.75	-1250	-5179.5
3D number of objects of 6 connectivity	5752	9606	536
3D number of objects of 18 connectivity	4293	7655	530
3D number of objects of 26 connectivity	4059	7293	528

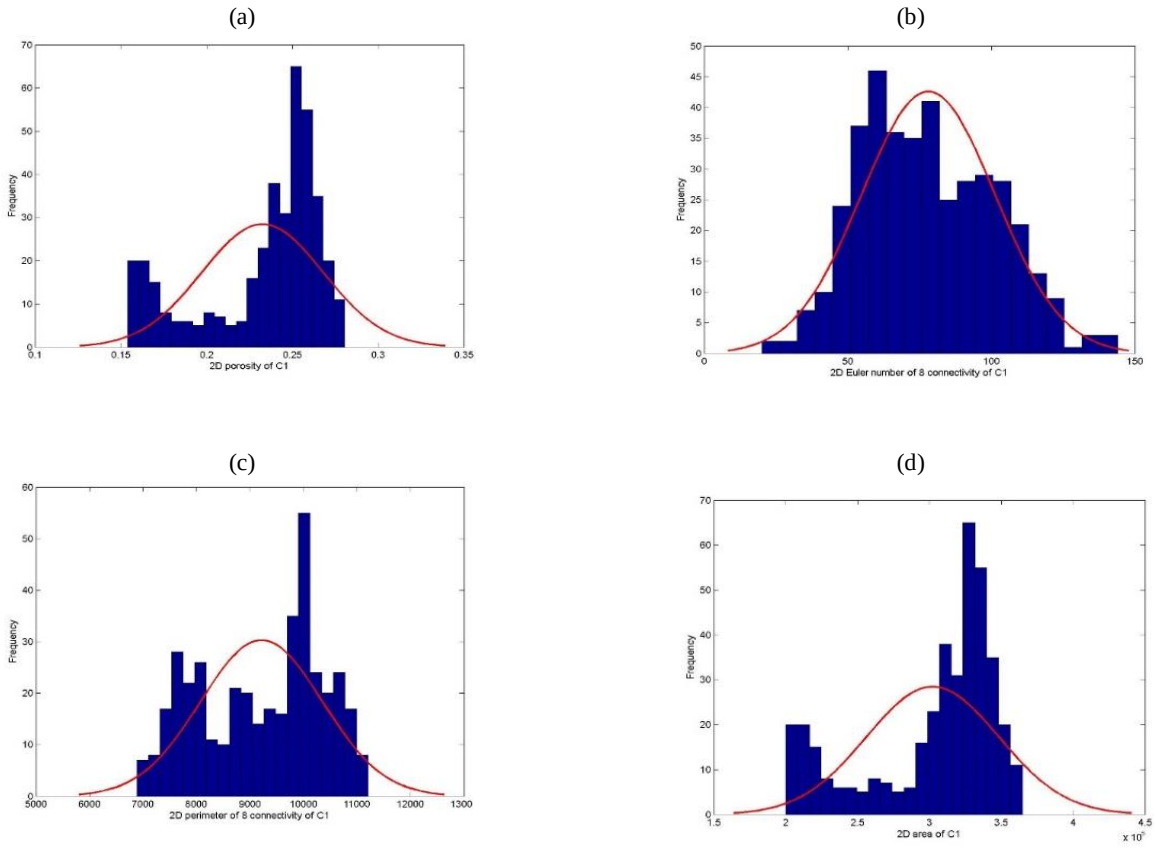

Fig. 10: 2D frequencies plots of (a) porosity, (b) Euler number, (c) perimeter, and (d) area for C1.

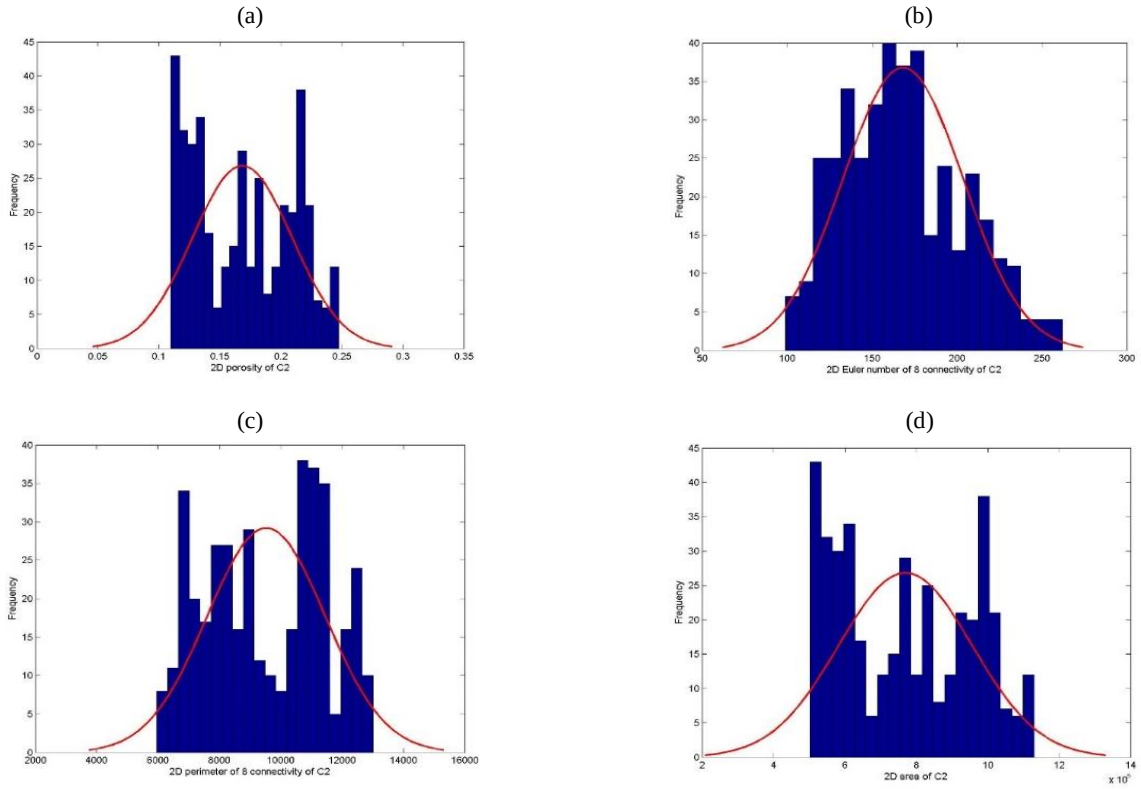

Fig. 11: 2D frequencies plots of (a) porosity, (b) Euler number, (c) perimeter, and (d) area for C2.

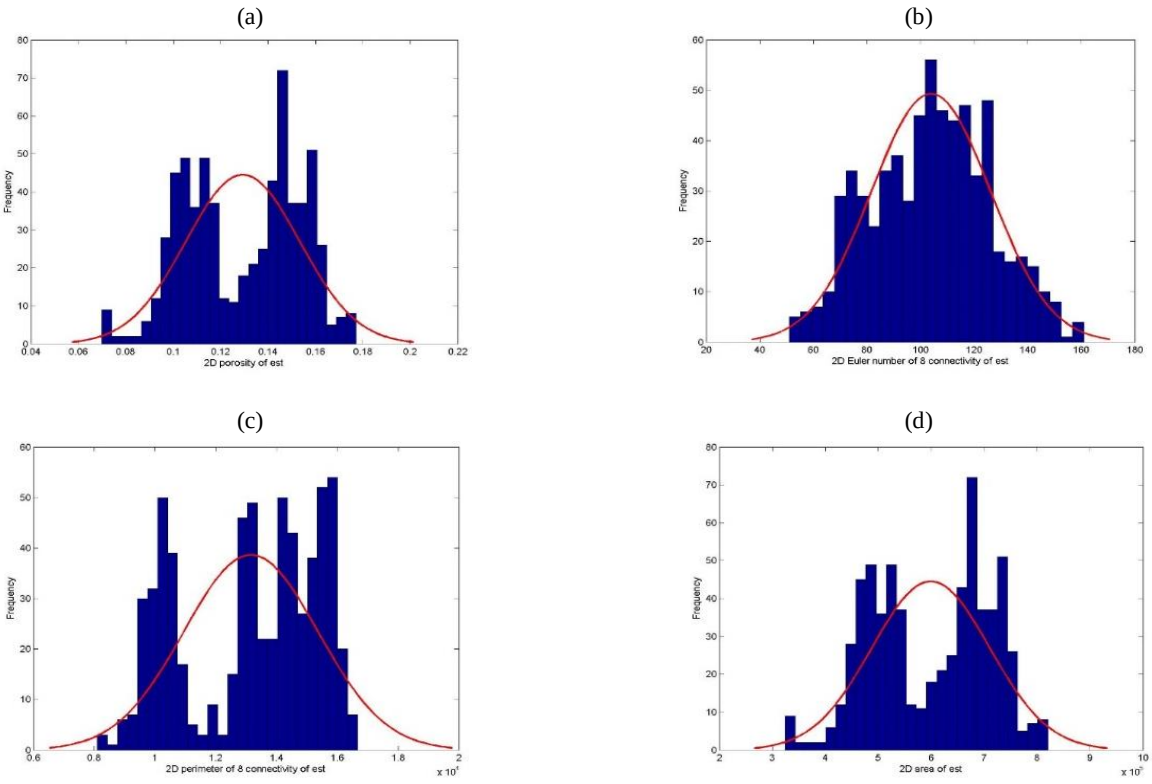

Fig. 12: frequencies plots of (a) porosity, (b) Euler number, (c) perimeter, and (d) area for Est.

CONCLUSIONS

The main idea of the present study was using two approaches for constructing the pore network in order to obtain the specifications of binary images of four carbonated rocks. The first approach, is the Rabbani's method, which is convenient regarding visualization of the network, but the pores are only considered as spheres. The second approach is to construct the pore network by using the skeletonization and skeleton to graph algorithms which have been introduced in separate works by Kollmannsberger.

The algorithms introduced by Kollmannsberger, originally proposed for bone image processing, were used for the first time in the present study for the construction of rock pore network.

The Kollmannsberger algorithms have the advantage that the pore shape is not limited to sphere. Considering the shortage of this method in visualizations, in contrast to Rabbani's method, this method has been improved in the present study to provide a convenient representation of the pore network. Here, the networks extracted by the improved Kollmannsberger method have been represented in this paper.

Also, in this research to obtain the specifications of binary images in addition to petrophysical properties, the geometrical properties have also been investigated through Minkowski functionals. Finally, using the properties extracted for the four carbonated rocks, the following findings have been obtained:

1- The porosity of the skeleton and the number of regions in dolomites are larger than those of limestones which is reasonable considering the usual higher porosities of dolomites.

2- The fewer the pores of carbonated rocks, the higher the average pore radius is.

3- The lower the variation in size of grains, the lower the number of throats is.

4- The lower the dolomite porosity, the lower the average throat length is.

5- There are fewer paths between the two opposite sides of the limestone network compared with the network extracted from dolomite.

6- As the permeability increases, the values of 2D geometrical properties increase, and the values of 3D geometrical properties decrease.

7- Inspecting the plots of frequencies for porosity, area and perimeter, it was found that there are two humps which indicates the double porosity behavior of carbonated rocks.

Nomenclatures

CT	Computed Tomography
2D	Two Dimensional
3D	Three Dimensional
SEM	Scanning Electron Microscopy
PCP	Pressure Controlled Porosimetry
RCP	Rate Controlled Porosimetry
NMR	Nuclear Magnetic Resonance
V	Vertices
E	Edges
F	Faces
S	Solids
#	Numbers
K	Absolute Permeability
Q	Flow
L	Length
A	Area
r	Effective Radius
R	Cylinder Radius
D	Grain Diameter
c	Constant
l_c	Characteristic Length
z	Critical Exponent
N	Grain Number
$\widehat{N}$	Effective Grain Number
S_0	Specific Surface Area
p	Empirical Parameter
C1	Sample Name
C2	Sample Name
Kett	Sample Name
Est	Sample Name
REV	Representative Elementary Volume

Greeks

χ	Euler Number
χ_0	Euler Number of Conducting Phase
α	Free Parameter
τ	Tortuosity
ϕ	Porosity
ϕ_c	Porosity at the Percolation Threshold
μ	Fluid Viscosity
σ	Conductivity
σ_0	Brine Conductivity

$\overline{\delta}$	Normalized Magnitude of Variation in Radius
$\overline{\lambda}$	Variation Wavelength
ΔP	Pressure Gradient

Received : Oct. 16, 2021 ; Accepted : Jan. 31, 2022

REFERENCES

[1] Lawrence M.A., David R.C., Characterization and Analysis of Porosity and Pore Structures. *Rev. Mineral. Geochem.*, **80(1)**: 61–164 (2015).

[2] Gao Z., Yang X., Hu C., Wei L., Jiang Z., Yang S., Fan Y., Xue Z., Yu H., Characterizing the Pore Structure of Low Permeability Eocene Liushagang Formation Reservoir Rocks from Beibuwan Basin in Northern South China Sea, *Mar. Petrol. Geol.*, **99**: 107–121 (2019).

[3] Hekmatzadeh M., Dadvar M., Emadi M., Experimental and Numerical Pore Scale Study of Residual Gas Saturation in Water/Gas Imbibition Phenomena, *Iran. J. Chem. Chem. Eng. (IJCCE)*, **34(3)**: 109-120 (2015).

[4] Kibria M.G., Hu Q., Liu H., Zhang Y., Kang J., Pore Structure, Wettability, and Spontaneous Imbibition of Woodford Shale, Permian Basin, West Texas, *Mar. Petrol. Geol.* **91**: 735–748, (2018).

[5] Shamsipur M., Bahrami Adeh N., Hajitarverdi M.S., Yazdimamagan M., Zarei F., Influence of Micro Silica a Mechanical Properties of Plasticized Sulfur Composites, *Iran. J. Chem. Chem. Eng. (IJCCE)*, **32(3)**: 1-7 (2013).

[6] Bartels W.B., Rücker M., Boone M., Bultreys T., Mahani H., Berg S., Imaging Spontaneous Imbibition in Full Darcy-Scale Samples at Pore-Scale Resolution by Fast X-Ray Tomography, *Water Resour. Res.*, **55**: 7072– 7085 (2019).

[7] Xiong Q., Jivkov A.P., Ahmad S.M., Modelling Reactive Diffusion in Clays with Two Phase-Informed Pore Networks, *Appl. Clay Sci.*, **119**, 222–228 (2016).

[8] Al-Kharusi A.S., Blunt M.J., Network Extraction from Sandstone and Carbonate Pore Space Images, *J. Pet. Sci. Eng.*, **56(4)**: 219–231 (2007).

[9] Piri M., Blunt M.J., Three-Dimensional Mixed-Wet Random Pore-Scale Network Modeling of Two-and Three-Phase Flow in Porous Media. I. Model Description, *Phys. Rev. E*, **71(2)**: 026301 (2005).

[10] Jiang Z., Wu K., Couples G., van Dijke M.J., Sorbie K.S., Ma J., Efficient Extraction of Networks from Three-Dimensional Porous Media, *Water Resour. Res.*, **43(12)**: (2007).

[11] Prodanović M., Lindquist W., Seright R., Porous Structure and Fluid Partitioning in Polyethylene Cores from 3D X-Ray Microtomographic Imaging, *J. Colloid Interface Sci.*, **298(1)**: 282–297 (2006).

[12] Legland D., Kieu K., Devaux M., Computation of Minkowski Measures on 2D and 3D Binary Images, *Image Anal. Stereol.*, **26(2)**: 83-92 (2007).

[13] Scholz C., Wirner F., Klatt M., Hirneise A., Schroder-Turk G.E., Mecke K., Bechinger C., Direct Relations Between Morphology and Transport in Boolean Models, *Phys. Rev. E*, **92**: 043023 (2015).

[14] Saxena N., Mavko G., Hofmann R., Srisutthiyakorn N., Estimating Permeability from Thin Sections Without Reconstruction: Digital Rock Study of 3D Properties from 2D Images, *Comput. Geosci.*, **102**: 79-99, (2017).

[15] Rabbani A., Jamshidi S., Salehi S., Determination of Specific Surface of Rock Grains by 2D Imaging, *J. Geol. Res.*, 945387 (2014).

[16] Kollmannsberger P., "Skeleton3D", MATLAB Central File Exchange, (2018)

[17] Kollmannsberger P., "Skel2Graph3D", MATLAB Central File Exchange, (2018)

[18] Raeini A.Q., Blunt M.J., Bijeljic B., Modelling Two-Phase Flow in Porous Media at the Pore Scale Using the Volume-of-Fluid Method, *J. Comput. Phys.*, **231(17)**: 5653-5668 (2013).

[19] Dong H., "Micro-CT Imaging and Pore Network Extraction. PhD, Department of Earth Science and Engineering", Imperial College London, (2008).

[20] Mostaghimi P., Bijeljic B., Blunt M.J., Simulation of Flow and Dispersion on Pore-Space Images, *SPE J.*, **17(04)**: - (2012).